

Axisymmetric spreading of a surfactant driven by self-imposed Marangoni stress under simplified transport

Shreyas Mandre

School of Engineering, Brown University, Providence RI 02912 USA

(Received xx; revised xx; accepted xx)

We numerically and theoretically calculate the steady flow driven by Marangoni stress due to surfactant introduced on a fluid interface at a constant rate. Two separate cases, where the surfactant either spreads in an adsorbed or in a dissolved phase are considered. We focus on the case where the size of the surfactant source is much smaller than the size of the fluid domain, and the resulting Marangoni stress overwhelms viscous forces so that the flow is strongest in a boundary layer close to the interface. The resulting flow in a region much larger than the surfactant source but smaller than the domain size is described by a self-similar profile. The radially outward component of fluid velocity decays with the radial distance r as $r^{-3/5}$ when the surfactant spreads in an adsorbed phase, and as r^{-1} when it spreads in a dissolved phase. Universal flow profiles that are independent of the system parameters emerge in both the cases.

1. Introduction

Surfactant spreading on a liquid has received much attention for thin films (Craster & Matar 2009), but not for deep layers of fluids. Past attempts at analyzing Marangoni-stress driven flow on a deep layer of fluid have been in the context of thermo-capillary (Bratukhin & Maurin 1967; Napolitano 1979; Zebib, Homsy & Meiburg 1985; Carpenter & Homsy 1990, e.g.) or thermo-solutocapillary convection (Bratukhin & Maurin 1968), with the notable exception of Jensen (1995) who analyzed transient dynamics from localized release of adsorbed surfactant. Interest has recently increased in the study of steady flow set by release of soluble amphiphiles (Young *et al.* 2009; Xu *et al.* 2013; Roché *et al.* 2014; Le Roux *et al.* 2016), in which case the surfactant transitions from an adsorbed phase to a dissolved phase. Consistent treatment of Marangoni-driven surfactant advection is of fundamental interest (Noskov 1996; Eastoe & Dalton 2000; Young *et al.* 2009; Xu *et al.* 2013).

Using a combination of numerical computations and analysis, we develop here the fundamental mathematical solutions describing the axisymmetric flow resulting from a concentrated steady source of surfactant on the surface of a deep fluid layer. We maintain the two-way coupling between the surfactant transport by the flow, and the fluid forcing by the surfactant. We focus on the case where the shear caused by the Marangoni stress drives a flow in a thin boundary layer near the fluid surface. Our main motivation and approach is to decompose the more general problem of soluble amphiphiles into two possibilities where the surfactant transport predominantly occurs in the adsorbed phase or the dissolved phase. Therefore, the two cases of adsorbed or dissolved surfactant are considered separately. Each case is simulated numerically (see §2.3) and the resulting flow in the region much larger than the surfactant source but much smaller than the flow domain is rationalized using similarity solutions (§3.1 and 3.2). The similarity solution for

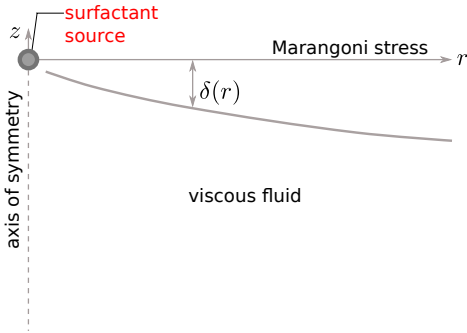


FIGURE 1. Schematic setup of the problem. A point source located at the origin releases insoluble surfactant on the interface of a semi-infinite pool of fluid. The interface is along the $z = 0$ plane. The Marangoni stress on the interface arising from the non-uniform distribution of surfactant drives a flow in a boundary layer of thickness $\delta(r)$.

dissolved surfactant is available due to Bratukhin & Maurin (1967), which we specialize to the limit where the flow occurs in a boundary layer. The similarity solution for the adsorbed surfactant is our own result.

2. Mathematical model

Consider an semi-infinite bath of fluid with a free interface along the $x - y$ plane as schematically shown in Figure 1. A surfactant is released at a constant rate from a point source located at the origin. The axisymmetric forcing suggests description of the flow in cylindrical polar coordinates (r, z) using the radial and axial components of velocity $u(r, z)$ and $w(r, z)$ respectively.

The fluid flow satisfies the incompressible Navier-Stokes equations

$$(ru)_r + rw_z = 0, \quad (2.1a)$$

$$(ru^2)_r + (rwu)_z + rp_r = \nu \left(ru_{zz} + (ru_r)_r - \frac{u}{r} \right), \quad (2.1b)$$

$$(ruw)_r + (rw^2)_z + rp_z = \nu (rw_{zz} + (rw_r)_r), \quad (2.1c)$$

where p is the fluid pressure field divided by fluid density. The fluid is quiescent far from the interface. The interface is assumed to be fixed at $z = 0$, and the Marangoni stress arising from the non-uniform surface tension σ implies

$$w = 0 \quad \text{and} \quad \mu u_z = \sigma_r \quad \text{at} \quad z = 0. \quad (2.2)$$

2.1. Case of insoluble surfactant

In the case of an insoluble surfactant, the surface tension σ depends on the area concentration of the surfactant c_2 , which we approximate as

$$\sigma = \sigma_0 - \Gamma_2 c_2, \quad (2.3)$$

where σ_0 is the interfacial tension without surfactant and Γ_2 is a material constant. We assume the Peclet number to be large, as is the case for most surfactants, so that diffusion of the surfactant can be neglected. The surfactant is transported along the interface by advection implying

$$2\pi ru(r, 0)c_2 = q_2 = \text{constant}, \quad (2.4)$$

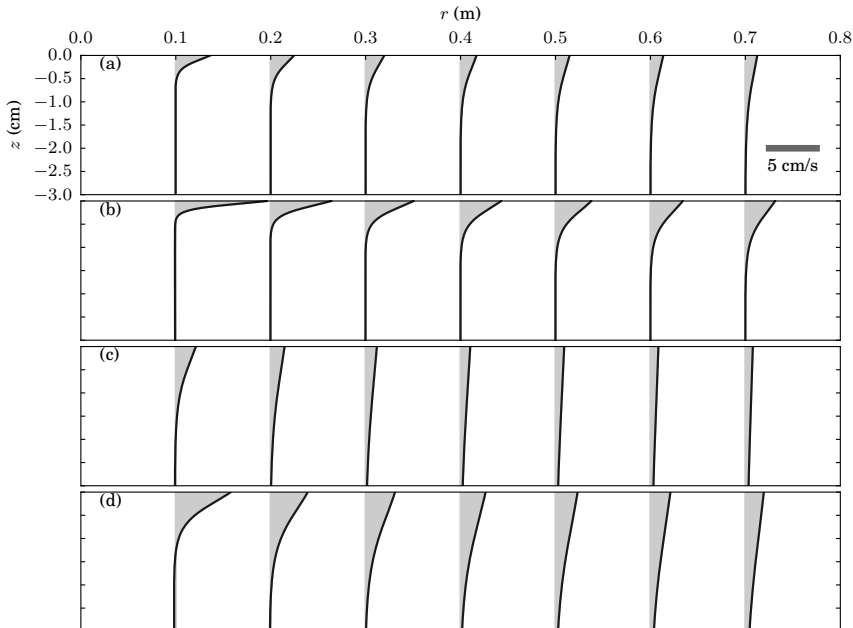


FIGURE 2. Sample radial velocity profiles near the free interface $z = 0$, where the strongest flow occurs, obtained from the solutions of (2.1-2.4). The profiles are plotted for 7 distances from the source corresponding to radial sections at $r=0.1, 0.2, 0.3, 0.4, 0.5, 0.6$, and 0.7 m as indicated by location of each curve. The four panels show: (a) $\nu = 10^{-6} \text{ m}^2/\text{s}$, $K_2 = 10^{-2} \text{ m}^3/\text{s}^2$, (b) $\nu = 10^{-6} \text{ m}^2/\text{s}$, $K_2 = 10^{-1} \text{ m}^3/\text{s}^2$, (c) $\nu = 10^{-5} \text{ m}^2/\text{s}$, $K_2 = 10^{-3} \text{ m}^3/\text{s}^2$, (d) $\nu = 10^{-5} \text{ m}^2/\text{s}$, $K_2 = 10^{-2} \text{ m}^3/\text{s}^2$.

where q_2 is the strength of the point source. Note that due to the linear relation between c_2 and σ in (2.3) and between c_2 and q_2 in (2.4), the parameters q_2 and Γ_2 only influence the flow through the combination $K_2 = \Gamma_2 q_2 / 2\pi\mu$. The only independent parameters in the problem are K_2 and ν , both possessing purely kinematic dimensions.

2.2. Case of soluble surfactant

In the case of a soluble surfactant, the volumetric concentration c_3 dominates surfactant transport and governs the surface tension profile, which we represent as

$$\sigma = \sigma_0 - \Gamma_3 c_3 \quad \text{at} \quad z = 0, \quad (2.5)$$

where Γ_3 is a material parameter. The surfactant, in this case, is transported within bulk of the fluid by an advection-diffusion process as

$$uc_{3,r} + wc_{3,z} = D \left[\frac{1}{r} (rc_{3,r})_r + c_{3,zz} \right], \quad (2.6)$$

where D is the diffusivity of the surfactant. Note that the bulk diffusivity of the surfactant may not be neglected in this case, even if the Peclet number is large. It is so because diffusion across the depth of the fluid layer governs the surface concentration, which in turn determines the Marangoni force. Conservation of the surfactant is expressed in terms of the integrated flux of surfactant q_3 crossing a cylinder of radius r as

$$\int_{-\infty}^0 [2\pi r u(r, z) c_3(r, z) - D r c_{3,r}(r, z)] dz = q_3 = \text{constant} \quad \text{for all } r. \quad (2.7)$$

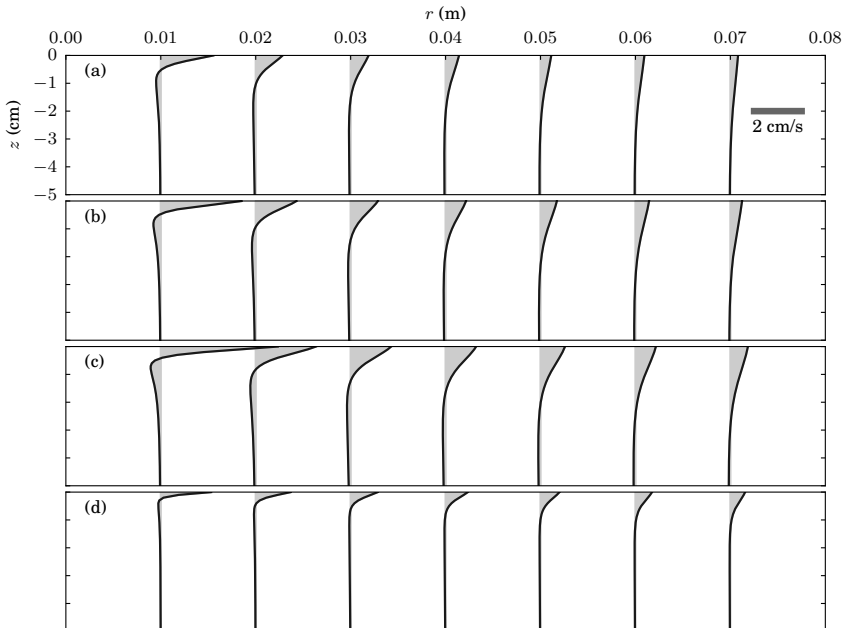


FIGURE 3. Sample radial velocity profiles near the free interface $z = 0$ obtained from the solutions of (2.1), (2.5), and (2.6). The profiles are plotted for 7 distances from the source corresponding to radial sections from $r=0.01$ to 0.07 m as indicated by location of each curve. The four panels show: (a) $K_3 = 4 \times 10^{-9} \text{ m}^4/\text{s}^2$, (b) $K_3 = 8 \times 10^{-9} \text{ m}^4/\text{s}^2$, (c) $K_3 = 16 \times 10^{-9} \text{ m}^4/\text{s}^2$, (d) $K_3 = 8 \times 10^{-9} \text{ m}^4/\text{s}^2$. Here $\nu = 2 \times 10^{-5} \text{ m}^2/\text{s}$, and $Sc = 2$, except for panel (d), where $\nu = 2 \times 10^{-6} \text{ m}^2/\text{s}$ and $Sc = 0.2$.

Similar to the case of insoluble surfactant, the linear relations between σ , c_3 and q_3 imply that Γ_3 and q_3 only appear in the combination $K_3 = \Gamma_3 q_3 / 2\pi\mu$. Thus K_3 , ν and D are the independent parameters describing the problem, all of them possessing purely kinematic dimensions.

2.3. Numerical solutions

Transient versions of the governing equations were implemented and solved using COMSOL's Computational Fluid Dynamics and Mathematical Modeling module starting from a static fluid layer with a clean interface until a steady state is reached. The domain was chosen to be a cylinder large enough (radius 2.5 m and depth 2.5 m for the insoluble case, and radius 0.48 m and depth 0.48 m for the soluble case) to approximate an infinite domain, but small enough so that for the parameters chosen no flow instabilities appeared. The $z < 0$ region of the cylinder is filled with a fluid possessing density in the range $10^3 - 10^4 \text{ kg/m}^3$ and dynamic viscosity μ ranging from $10^{-1} - 10^{-3} \text{ Pa s}$. The point source of surfactant located at the origin is assigned a small finite extent (radial extent $r_0 \approx 5 \times 10^{-4} \text{ m}$) so that the singularity at $r = 0$ is regularized. Outflow (i.e. zero gage pressure) boundary conditions are imposed at the outer radius and lower boundary to better approximate an infinite domain. We also ensured that imposing other boundary conditions such as no-slip or slip without penetration does not significantly affect the flow in the region much larger than r_0 but smaller than the domain size. We used a non-uniform unstructured triangular mesh and a non-uniform structured rectangular mesh for discretization. The discretization is finer near the surfactant source and the interface

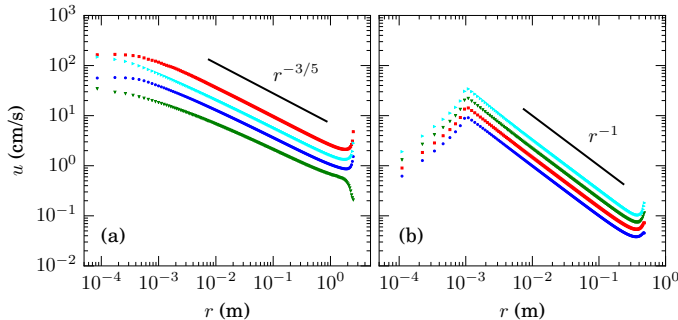


FIGURE 4. (Colour online) Surface radial velocity as a function of radial distance. (a) The four cases of insoluble surfactant shown in Figure 2. Solid black line shown the power law $r^{-3/5}$. (b) The four cases of soluble surfactant shown in Figure 3. Solid black line shown the power law r^{-1} .

to resolve the presence of the boundary layer. The grid was successively refined to test for numerical convergence and confirm the self-similar flow structure.

Sample steady state radial flows for four cases are shown in Figure 2 and 3. The flow is fastest at the interface, and falls off rapidly with depth over a length of $O(1 \text{ cm})$ indicating a boundary layer structure driven by Marangoni stresses. Comparison between Figure 2(a-b) and (c-d) shows that the surface flow increases and the apparent boundary layer thickness decreases with increasing insoluble surfactant source strength, K_2 . Similarly, Figure 3(a-c) shows such behaviour for soluble case with parameter K_3 . In both cases, the surface flow decreases and the apparent boundary layer thickness increases with increasing kinematic viscosity ν , as can be seen by comparing panels (a,c) with (b,d) of Figure 2, and panels (b) with (d) of Figure 3. The observations will be explained using a boundary layer approximation and self-similar solution of the governing equations.

A simple description of the flow in terms of power law decay away from the surfactant source may be derived using dominant balances as follows. At a radius r from the source, let us assume that the radial velocity decays as a power law denoted by $u(r)$ and the surfactant concentration as $c_{2,3}(r)$. A balance between inertia (per unit mass) which scales as u^2/r and viscous forces which scale as $\nu u/\delta^2$, where $\delta(r)$ is the expected boundary layer thickness, implies $\delta = (\nu r/u)^{1/2}$. When the surfactant spreads in an adsorbed phase, its conservation implies $2\pi r u c_2 = q_2$. Combining this with a balance between the Marangoni stress $\Gamma_2 c_2/r$ and the shear stress on the interface $\mu u/\delta$, yields

$$u \propto \frac{K_2^{2/5} \nu^{1/5}}{r^{3/5}}, \quad \delta \propto \frac{\nu^{2/5} r^{4/5}}{K_2^{1/5}}, \quad \text{and} \quad \frac{c_2}{q_2} \propto \frac{1}{K_2^{2/5} \nu^{1/5} r^{2/5}}. \quad (2.8)$$

A similar scaling analysis for the case of dissolved surfactant may be used to rationalize the r^{-1} scaling of velocity but not the dimensional pre-factor. It can readily be seen from momentum conservation that if $u \propto r^n$, then $\delta \propto r^{(1-n)/2}$. Surfactant transport occurs in a layer of thickness $\delta \text{Sc}^{-1/2} \propto r^{(1-n)/2}$. The Marangoni stress at the surface scales as $u/\delta \propto r^{(3n-1)/2}$, which implies the surfactant concentration scales as $c_3 \propto r^{(3n+1)/2}$. Therefore, the surfactant flux is $q_3 \propto r u c_3 \delta \propto r^{2(1+n)}$. Since q_3 is independent of r , we conclude $n = -1$, implying $u \propto r^{-1}$, $\delta \propto r$, and $c_3 \propto r^{-1}$. The reason for the failure of this simple scaling argument to yield the dimensional pre-factors will be clarified later.

In Figure 4, we plot the numerically obtained radial velocity on the surface as a function of r and compare it with the afore-derived power laws. The power-law behavior compares

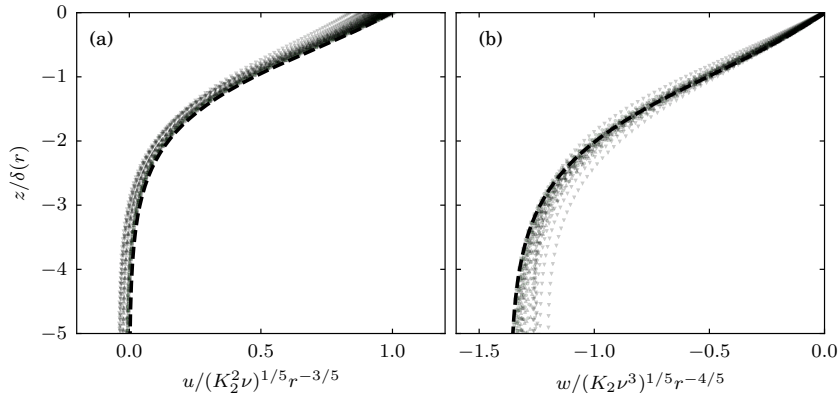


FIGURE 5. (Colour online) Comparison of the computational solutions with the similarity solution for the case of adsorbed surfactant transport. (a) The radial component and (b) the axial component of fluid velocity, scaled according to the similarity solution predictions, is plotted (green symbols) for all the profiles shown in Figure 2. The solution of (3.5-3.7) obtained using shooting method (dashed curve) is also shown for comparison.

well with the numerical solution in an intermediate range of radial distances, which are much larger than the source but smaller than the domain size.

3. Self-similar profiles

The power-law description paves way for a self-similar description of the flow in this intermediate region, which we derive next. The simple balances presented above, including the dimensional pre-factors for the adsorbed surfactant case, are closely associated with a self-similar flow with a universal velocity and surfactant profile, which is the topic of the rest of the article.

3.1. Adsorbed surfactant

The power law in the surface velocity profile implies scale free dynamics, and therefore a self-similar flow. The self-similar flow can be described using a similarity variable

$$\xi = \frac{z}{\delta(r)}, \text{ where } \delta = \frac{\nu^{2/5} r^{4/5}}{K_2^{1/5}} \quad (3.1)$$

is the boundary layer thickness according to (2.8). Assuming $\delta \ll r$, the governing fluid equations simplify to the Prandtl boundary layer equations

$$uu_r + ww_z = \nu u_{zz}, \quad p_z = 0, \quad (ur)_r + rw_z = 0, \quad (3.2)$$

in a region of length $O(\delta)$ near the interface. Outside this region, the flow is weak, and therefore approximated as $u = w = p = 0$.

Continuity (2.1c) may be satisfied by using a self similar form for the stream function with the dimensional pre-factor determined from (2.8) as

$$ru = \psi_z, \quad rw = -\psi_r, \quad \psi(r, z) = K_2^{2/5} \nu^{1/5} r^{2/5} \delta(r) f(\xi), \quad (3.3)$$

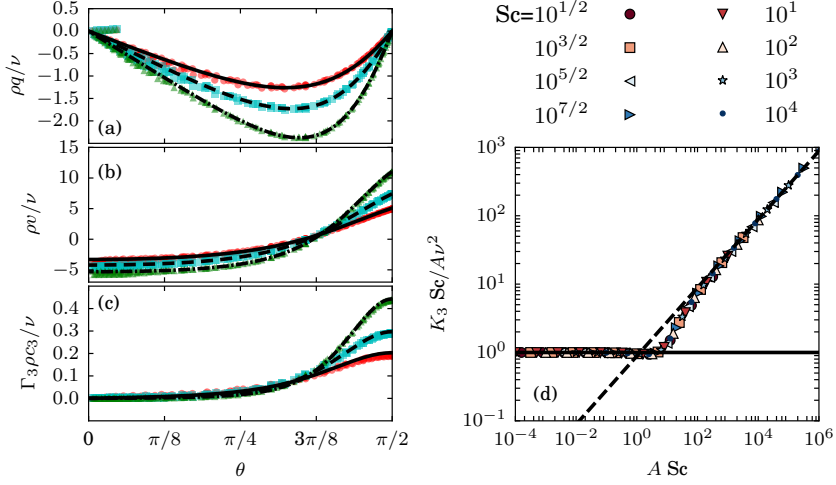


FIGURE 6. (Colour online) Similarity solution for the case of soluble surfactant and comparison with rescaled computational results from Figure 3(a-c). (a) Radial velocity, (b) azimuthal velocity, and (c) surfactant concentration. Symbols indicate results of rescaled computational solutions $K_3 Sc/\nu^2 = 20$ (red circles), 40 (cyan squares), and 80 (green triangles) corresponding to panels in Figure 3 (a-c) respectively. Black curves indicate similarity solutions corresponding to $K_3 Sc/\nu^2 = 20$ (solid), 40 (dashed), and 80 (dot-dashed). (d) Relation between A and the strength of Marangoni stress quantified by a single parameter $K_3 Sc/\nu^2 A$ from (3.11) for different Sc . The solid line shows the asymptotic value $K_3 Sc/\nu^2 A = 1$ for $A \ll 1$ and the dashed line shows $K_3 Sc/\nu^2 A = (\pi Sc A)^{1/2}/2$ for $A \gg 1$.

where f is function to be determined. According to this ansatz,

$$u(r, z) = \frac{K_2^{2/5} \nu^{1/5}}{r^{3/5}} f'(\xi), \quad \text{and} \quad w(r, z) = -\frac{K_2^{1/5} \nu^{3/5}}{5r^{4/5}} (6f(\xi) - 4\xi f'(\xi)). \quad (3.4)$$

Substituting this ansatz in (3.2) yields

$$f'''(\xi) + \frac{3}{5} f'(\xi)^2 + \frac{6}{5} f(\xi) f''(\xi) = 0. \quad (3.5)$$

The boundary conditions (2.2), (2.3) and (2.4) can be combined into one by eliminating $c_2(r)$, to get

$$u_z(r, z=0) = -\frac{\Gamma_2 q_2}{2\pi\mu} \left(\frac{1}{ru(r, 0)} \right)_r = -K_2 \left(\frac{1}{ru(r, 0)} \right)_r. \quad (3.6)$$

Upon substitution of the ansatz (3.4) in (3.6), the condition (2.2), and the stagnation of the fluid outside the boundary layer yields a full set of boundary conditions for f as

$$f(0) = 0, \quad f''(0)f'(0) = \frac{2}{5}, \quad \text{and} \quad f'(-\infty) = 0. \quad (3.7)$$

The simple dominant balance, which we used to derive the power-law expressions in (2.8), can be seen throughout this derivation as the balance between coefficients of the terms representing the respective physical effects. In this manner, the simple dominant balance analysis represents the more detailed derivation based on self-similarity.

Equations (3.5-3.7) are numerically solved using a shooting method, which we outline next. The method starts with a guess for $f''(0)$ and sets the corresponding $f'(0)$ using

(3.7). The initial value problem with the guessed initial condition is then solved numerically using a fourth order Runge Kutta method and its asymptotic behavior as $\xi \rightarrow -\infty$ is examined. The solution asymptotically either diverges to ∞ or $-\infty$ as $f \sim C\xi^{2/3}$, thereby violating the far-field boundary condition in (3.7). However, between the cases that diverge to ∞ and those that diverge to $-\infty$ is one solution that remains bounded. For this case f approaches a constant values, f_∞ . This possibility may be examined by making the ansatz $f = f_\infty + \epsilon g(\xi) + \dots$ for $\epsilon \ll 1$, resulting in

$$f(\xi) = f_\infty + \epsilon \left(a_1 + b_1 \xi + c_1 e^{-6f_\infty \xi/5} \right) + O(\epsilon^2), \quad (3.8)$$

where a_1 , b_1 and c_1 represent arbitrary constants of integration. Note that b_1 must be zero so that asymptotic ordering of the solution is maintained as $\xi \rightarrow -\infty$ and a_1 may be absorbed into f_∞ . The objective of the shooting method is to guess the initial value $f''(0)$ such that this bounded solution with $b_1 = 0$ is asymptotically achieved. We find this solution by successive bisection of the interval of $f''(0)$ with end points that lead to diverging solutions with opposite signs. This bisection was implemented manually to determine that $f''(0) = 0.402287361293201$ solves (3.5-3.7) numerically to 15 digit accuracy. The resulting self-similar profile for u and w based on the solution for $f(\xi)$ and its derivatives is shown in Figure 5.

The similarity solution is compared with the four direct computational solution in Figure 5. The reduction of the variability between the profiles resulting from the differences in K_2 , ν , and r , and the excellent comparison with the $f(\xi)$ and its derivatives computed as a solution of (3.5) and (3.7), verifies the validity of the similarity solution.

3.2. Dissolved surfactant

The boundary layer approximation, that so successfully describes the flow resulting in the case of surfactant transported in the adsorbed phase, fails for the case of dissolved surfactant. The reason for this failure will be presented later. However, a self-similar solution is still possible, as first demonstrated by Bratukhin & Maurin (1967). Here we present a comparison of their solution with our numerical results. In addition, we derive the asymptotic behavior of this solution in the physically relevant limit of $Sc = \nu/D \gg 1$ and show that a universal self-similar profiles exist in the limit $K_3 Sc/\nu^2 \gg 1$.

The solution is best presented in terms of spherical polar coordinates (ρ, θ) defined by $r = \rho \sin \theta$ and $z = -\rho \cos \theta$, with the corresponding velocity components v and q respectively. The self-similar ansatz in this case is

$$v = \nu \frac{f(\theta)}{\rho}, \quad q = \nu \frac{g(\theta)}{\rho}, \quad \text{and} \quad c_3 = \frac{\nu}{\Gamma_3} \frac{h(\theta)}{\rho}, \quad (3.9)$$

in terms of the recycled symbols f , g and h . An exact solution of the Navier-Stokes equations is possible in this case, represented in terms of a single parameter A as

$$g(\theta) = -2 \frac{d}{d\theta} \log F(\zeta), \quad f(\theta) = -\frac{1}{\sin \theta} \frac{d}{d\theta} (\sin \theta g(\theta)), \quad h(\theta) = \frac{\mu A (1 + A)^{Sc}}{F(\zeta)^{2Sc}}, \quad (3.10a)$$

$$\text{where } \zeta = 1 + \cos \theta, \quad F(\zeta) = n_2 \zeta^{n_1} - n_1 \zeta^{n_2}, \quad \text{and} \quad n_{1,2} = \frac{1 \pm \sqrt{1 + A}}{2}. \quad (3.10b)$$

The parameter A quantifies the strength of the Marangoni forcing (the surface velocity is $A\nu/2r$) and is related to the surfactant release rate by

$$\frac{K_3 Sc}{\nu^2} = A(1 + A)^{Sc} \int_1^2 \left[4Sc^2 \zeta (2 - \zeta) \frac{F'(\zeta)^2}{F(\zeta)^2} + 1 \right] \frac{d\zeta}{F(\zeta)^{2Sc}}. \quad (3.11)$$

The results of the numerical solutions shown in Figure 3, when rescaled according to the self-similar ansatz, collapse on the similarity solution (3.10a), as shown in Figure 6. Note that, while the flow is self-similar, the profile shape is not universal, but varies with A , which depends on the strength of Marangoni stress as represented by $K_3\text{Sc}/\nu^2$ and Sc . This dependence is shown in Figure 6(d), for Sc from $\sqrt{10}$ to 10^6 , the range of Sc that encompasses many common chemical species. This range of Sc corresponds to the asymptotic limit $\text{Sc} \gg 1$. This dependence from (3.11) has the asymptotic limits

$$A \sim K_3\text{Sc}/\nu^2 \text{ for } A \ll 1 \quad \text{and} \quad A \sim \frac{2^{2/3}K_3^{-2/3}\text{Sc}^{1/3}}{\pi^{1/3}\nu^{4/3}} \text{ for } A \gg 1. \quad (3.12)$$

In these two extremes, we expect a universal flow profile to emerge. In the case we are interested where $A \gg 1$, the solution (3.10a) simplifies in a region of thickness $\Delta n z = O(1)$ (transforming to cylindrical polar coordinates) to

$$u(r, z) \approx \frac{A\nu}{2r} e^{z/r} \left\{ \frac{\cosh(\Delta n^{-1})}{\cosh^2(\hat{\xi} - \Delta n^{-1})} - 2\Delta n^{-1} \frac{\sinh(\hat{\xi})}{\cosh(\hat{\xi} - \Delta n^{-1})} \right\} + O(\Delta n^{-2}), \quad (3.13)$$

where $\hat{\xi} = \Delta n z / 2r$, A and $\Delta n = \sqrt{1 + A}$ are determined from (3.11) (or Figure 6(d)). In the limit of large A , the profile approaches

$$u(r, z) \approx \frac{A\nu}{2r} \text{sech}^2\left(\frac{zA^{1/2}}{2r}\right) + O\left(\frac{1}{\Delta n}\right). \quad (3.14)$$

Varying A in (3.14) simply rescales the boundary layer thickness as $\delta = 2r/A^{1/2}$ and the velocity magnitude as A , but does not change the shape of the profile. In this sense, the profile is universal. However, note that the leading order approximation in (3.14) fails to support any shear at $z = 0$, and is therefore incapable of transmitting the Marangoni stress from the surfactant. The flow profile in (3.14) in fact describes a free radial jet forced by a steady point momentum source at the origin and a shear free boundary condition on the surface. A solution of Prandtl's boundary layer approximation that decays as $1/r$ simply yields this radial jet, as originally derived by Squire (1955), and fails to match the Marangoni stress condition. Bratukhin and Maurin's solution is a perturbation of Squire's jet, where the Marangoni stress is supported by the next term of $O(\Delta n^{-1})$, and therefore the surface shear stress does not scale with dimensional parameters according to the leading order. Due to this structure of the flow, the simple scaling analysis of the type presented in §2.3 fails to capture the dependence of dimensional pre-factors on the parameters. Using the next order correction in (3.13) or the complete solution in (3.10a), we see that the shear at the surface is $A\nu/r^2$ (weaker than the dimensionally expected $A\nu/\delta r$ as explained). The shear stress on the surface $\mu A\nu/r^2$ thus balances the Marangoni stress, which scales as $\Gamma_3 c_3/r$, yielding the scale for surfactant concentration $c_3 \propto \mu A\nu/\Gamma_3 r$. Surfactant transport rate q_3 then scales as $r u c_3 \delta \text{Sc}^{-1/2} = A^{3/2} \nu^2 \mu / \Gamma_3 \text{Sc}^{1/2}$, where we have used that the surfactant boundary layer is thinner than the momentum boundary layer by a factor $\text{Sc}^{1/2}$. This final balance yields $A \propto (K_3^2 \text{Sc} / \nu^4)^{1/3}$ in agreement with (3.12) and the results in Figure 6(d).

4. Conclusion

Here we have presented the similarity solutions underlying the Marangoni stress driven flow due to a point source of surfactant, as it spreads either in an adsorbed or dissolved

state. The scope of this paper is limited to the case where the flow occurs in a thin layer close to the free surface, as characterized by $\delta \ll r$ for both cases, which in either case results in a universal velocity profile. The radial component of velocity decays as $r^{-3/5}$ in the adsorbed case and as r^{-1} in the dissolved case. The similarity solution for the case of the adsorbed surfactant is derived using Prandtl's boundary layer approximation. For $K_3\text{Sc}/\nu^2 \gg 1$ and $\text{Sc} \gg 1$, a universal boundary layer profile (3.14) emerges.

Our results rationalize experimental observations of the power-law decay and boundary layer structure of Marangoni-driven flow (Mandre, Akella, Singh, Singh & Bandi 2017). The agreement between the experimental measurements and our theory suggests that the more general surfactant dynamics may under certain circumstances be reduced to simple models. The solutions developed here could also be used as building blocks to rationalize flow structures that arise when the surfactant actively transitions from adsorbed to dissolved phases (Roché *et al.* 2014; Le Roux *et al.* 2016), and deduce relevant material parameters. The precise criteria under which simplification is possible and conditions for transition are left to be undertaken in the future.

REFERENCES

- BRATUKHIN, I. K. & MAURIN, L. N. 1967 Thermocapillary convection in a fluid filling a half-space: PMM vol. 31, no. 3, 1967, pp. 577–580. *Journal of Applied Mathematics and Mechanics* **31** (3), 605–608.
- BRATUKHIN, Y. K. & MAURIN, L. N. 1968 Dissolution of a hot body in contact with a free liquid surface. *Journal of Engineering Physics and Thermophysics* **14** (6), 533–535.
- CARPENTER, B. M. & HOMSY, G. M. 1990 High Marangoni number convection in a square cavity: Part II. *Physics of Fluids A: Fluid Dynamics* **2** (2), 137–149.
- CRASTER, R. V. & MATAR, O. K. 2009 Dynamics and stability of thin liquid films. *Reviews of modern physics* **81** (3), 1131.
- EASTOE, J. & DALTON, J. S. 2000 Dynamic surface tension and adsorption mechanisms of surfactants at the air–water interface. *Advances in colloid and interface science* **85** (2), 103–144.
- JENSEN, O. E. 1995 The spreading of insoluble surfactant at the free surface of a deep fluid layer. *Journal of Fluid Mechanics* **293**, 349–378.
- LE ROUX, S., ROCHÉ, M., CANTAT, I. & SAINT-JALMES, A. 2016 Soluble surfactant spreading: How the amphiphilicity sets the Marangoni hydrodynamics. *Physical Review E* **93** (1), 013107.
- MANDRE, S., AKELLA, V. S., SINGH, D. K., SINGH, R. S. & BANDI, M. M. 2017 Hydrodynamic signature of Marangoni-driven surfactant transport dominated by adsorbed versus dissolved phase. *in preparation*.
- NAPOLITANO, L. G. 1979 Marangoni Boundary Layers. *Proceedings of 3rd European Symposium on Material Sciences in Space* **SP-142**, 349–358.
- NOSKOV, BA 1996 Fast adsorption at the liquid-gas interface. *Advances in colloid and interface science* **69** (1-3), 63–129.
- ROCHÉ, M., LI, Z., GRIFFITHS, I. M., LE ROUX, S., CANTAT, I., SAINT-JALMES, A. & STONE, H. A. 2014 Marangoni flow of soluble amphiphiles. *Physical Review Letters* **112** (20), 208302.
- SQUIRE, H. B. 1955 Radial jets. *Fifty Years of Boundary Layer Research* pp. 47–54.
- XU, K., BOOTY, M. R. & SIEGEL, M. 2013 Analytical and computational methods for two-phase flow with soluble surfactant. *SIAM Journal on Applied Mathematics* **73** (1), 523–548.
- YOUNG, Y-N, BOOTY, M. R., SIEGEL, M. & LI, J. 2009 Influence of surfactant solubility on the deformation and breakup of a bubble or capillary jet in a viscous fluid. *Physics of Fluids* **21** (7), 072105.
- ZEBIB, A., HOMSY, G. M. & MEIBURG, E. 1985 High Marangoni number convection in a square cavity. *The Physics of fluids* **28** (12), 3467–3476.